Polyhedron 176 (2020) 114275

Contents lists available at ScienceDirect

Polyhedron

journal homepage: www.elsevier.com/locate/poly

Feasibility of ground state spin switching in a molecular analogue of the mixed-metal oxides with the perovskite structure ☆

Thai Son Cao [a], Dian-Teng Chen [b], Khalil A. Abboud [a], Xiaoguang Zhang [b], Hai-Ping Cheng [b], George Christou [a,*]

[a] Department of Chemistry, University of Florida, Gainesville, FL 32611, USA
[b] Department of Physics, University of Florida, Gainesville, FL 32611, USA

ARTICLE INFO

Article history:
Received 13 October 2019
Accepted 4 December 2019
Available online 11 December 2019

Keywords:
Manganese
Cerium
Cluster
Crystal structure
Magnetism

ABSTRACT

The carboxylate substitution reaction between the reported all-benzoate complex $[Ce_3Mn_8O_8(PhCO_2)_{18}(PhCO_2H)_2]$ (**1**) and 2-Cl-benzoic acid has led to isolation of $[Ce_3Mn_8O_8(2\text{-}Cl\text{-}PhCO_2)_{15.3}(PhCO_2)_{2.7}(H_2O)_2]$ (**2**). The structures of **1** and **2** are very similar, both containing a tetragonally-elongated Mn_8^{III} cuboid with a Ce^{IV} at its center and two Ce^{III} attached to opposite faces, but **2** shows extensive disorder in the ligands and the Cl atom positions and occupancies. Variable-temperature (T) solid-state dc and ac magnetic susceptibility data for **2** are significantly different from those for **1** and are assigned as due to small ligand-induced structural perturbation of the core that has brought an **A-type antiferromagnetic (AF)** excited state much closer to the **C-type AF** ground state. Fits of the dc $\chi_M T$ vs T data support this interpretation but due to the ligand disorder in **2**, a more definitive description of the lowest energy spin states of **2** is not possible. Nevertheless, these results provide important support for the feasibility of ground state spin switching by ligand-induced core perturbation ('chemical pressure') in this family, and they encourage further studies.

1. Introduction

A recent interest in our group is the application of a molecular bottom-up approach to ultra-small (<10 nm) nanoparticles of important metal oxides, both homo- and heterometallic. This brings to this field all the advantages of molecular chemistry, particularly truly monodisperse (single-size) materials that are also of identical shape, solubility, and crystallinity, the latter also allowing structural characterization to atomic resolution by single-crystal X-ray crystallography. We now call such species "molecular nanoparticles", and the *sine qua non* of this approach is that the molecular species must have the same M/O structure as the bulk metal oxide, otherwise they cannot be considered their nanoparticles but instead just new M/O clusters. In our work targeting molecular nanoparticles of CeO_2, an important material with a wide range of catalytic uses spanning industrial, environmental and biomedical catalysis [1–5], we recently reported a family of molecular species with the same Ce/O fluorite structure as the bulk material and with Ce nuclearities up to 40 [6]. Similarly, we also reported the cluster $[Ce_3Mn_8O_8(PhCO_2)_{18}(PhCO_2H)_2]$ (**1**), whose structure can be described as comprising one whole and two half repeating units of the $AMnO_3$ (A = lanthanide or main group metal) manganite perovskites [7] and which has a so-called **C-type** antiferromagnetic (**AF**) ground state, one of the common spin configurations seen in magnetic perovskites (scheme 1). The present work is an extension of this perovskite-related project.

We were interested to see that theoretical computations on $LaMnO_3$, which has an **A-type AF** ground state, had predicted that small changes to the weak **AF** interactions between Mn^{III} ions arising from overlap of their d_π (t_{2g}) magnetic orbitals could lead to ground state spin switching to any of the others in the scheme [8,9]. DFT studies also predicted that changes to certain lattice parameters of $LaMnO_3$ would result in a change in its spin state [10,11]. Attempts to demonstrate this experimentally by applying pressure to $LaMnO_3$ gave no change up to 7 GPa, and higher pressures up to 15 GPa led to a higher symmetry phase in which the Mn^{III} Jahn-Teller distortions were lost [12,13], making the theoretical predictions no longer valid. A colossal magnetoresistance study under ultra-high pressure up to 46 GPa, however, suggested that a lattice compression in $LaMnO_3$ can induce small ferromagnetic domains [14]. Since weak exchange interactions in molecular

☆ Dedicated to the founding in 2019 of the annual *Molecular Magnetism in North America* (MAGNA) workshop.

* Corresponding author.
E-mail address: christou@chem.ufl.edu (G. Christou).

https://doi.org/10.1016/j.poly.2019.114275
0277-5387/

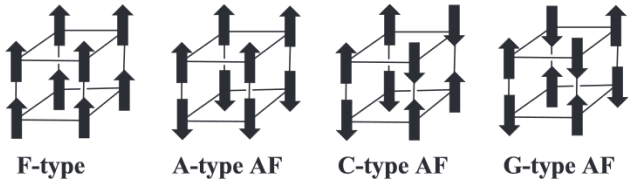

Scheme 1. Common spin vector orderings in magnetic perovskites.

species are often sensitive to small ligand-induced structural distortions, we wondered whether introducing substituents into the benzoate *ortho* position might induce small structural perturbations from the resulting 'chemical pressure' on the core, and possibly switch the ground state. We were encouraged in this belief by the results of DFT calculations on **1** that showed that the first two excited states are **A-type AF** and fairly close in energy to the ground state. We were also encouraged by our previous work with other cluster types where we had successfully switched the ground state using such a ligand-induced chemical pressure strategy [15–17].

We herein report the synthesis, structure, and magnetic properties of a derivative of **1** prepared using 2-Cl-benzoic acid, and our assessment of whether changes to the ground state of this Ce_3Mn_8 cluster family is a possibility.

2. Experimental

2.1. Synthesis of $[Ce_3Mn_8O_8(2\text{-}Cl\text{-}PhCO_2)_{15.3}(PhCO_2)_{2.7}(H_2O)_2]$ (**2**)

To a stirred solution of 2-Cl-$PhCO_2H$ (2.57 g, 16.4 mmol) in MeCN (20 mL) at 55 °C was added solid $Mn(PhCO_2)_2$ (0.700 g, 2.05 mmol) to give a light pink solution. After 5 mins, $Ce(NO_3)_3{\cdot}4H_2O$ (0.910 g, 2.05 mmol) was added to give on dissolution a deep red solution, and then solid $N^nBu_4MnO_4$ (0.19 g, 0.53 mmol) was added in small portions. The resulting dark brown solution was stirred at 55 °C for another 1 h and then filtered while hot. The filtrate was left to cool to room temperature and then maintained undisturbed at ambient temperature. The next day it was filtered again to remove a small amount of powder that had formed. After another 5 days undisturbed, the X-ray quality brown plate-like crystals of **2**·$^5/_2$MeCN that had grown were collected by filtration, washed with Et_2O, and dried under vacuum. The yield was 21% based on Mn. *Anal.* Calc. (Found) for solvent-free **2** ($C_{126}H_{78.7}Ce_3Cl_{15.3}Mn_8O_{46}$): C, 40.56 (40.35); H, 2.13 (1.99); N, 0.00 (0.00); Cl, 14.54 (14.35). Selected IR data (cm^{-1}): 3431 (w), 3132 (w), 1610 (s), 1591 (s), 1549 (s), 1507 (w), 1473 (m), 1401 (s), 1280 (w), 1261 (w), 1158 (m), 1125 (m), 1053 (m), 1040 (m), 989 (w), 957 (w), 844 (w), 801 (w), 748 (s), 720 (m), 685 (m), 649 (m), 607 (m), 579 (m), 532 (m), 458 (w).

2.2. X-ray crystallography

Data for **2**·$^5/_2$MeCN were collected on a Bruker DUO diffractometer at 100 K using MoK$_\alpha$ radiation (λ = 0.71073 Å). A single crystal of the sample was kept in silicone grease and mounted on a measuring tip, where it was cooled to 100 K. An APEXII CCD area detector was used to collect diffracted signals. Raw data were read by program SAINT [18]. The structures were solved by direct methods with program *SHELXTL2014* [19] and refined on F^2 by full-matrix least-squares cycles. The non-H atoms were refined anisotropically, and H atoms were placed in calculated, idealized positions and refined as riding on their parent atoms. The asymmetric unit contains the complete Ce_3Mn_8 cluster and four MeCN solvent molecules with 100:50:50:50% occupancies. Every Ph ring has a Cl atom attached, and all resulting 2-Cl-Ph rings are disordered about two positions and/or have partial Cl occupancy. The total Cl occupancy in the molecule corresponds to 15.3 Cl atoms, in agreement with the Cl elemental analysis and the molecular formula (vide supra). The refinement was carried out by minimizing the wR_2 function using F^2 rather than F values. R_1 is calculated to provide a reference to the conventional R-value, but its function is not minimized. In the final cycle of refinement, 32,585 reflections (of which 19,507 were observed with $I > 2\sigma(I)$) were used to refine 1736 parameters, yielding R_1, wR_2 and S of 8.06%, 18.42% and 1.060, respectively. Unit cell data and structure refinement details are collected in Table 1.

2.3. Physical measurements

Infrared spectra were recorded in the solid-state (KBr pellets) on a Thermo Scientific Nicolet iS5 FTIR spectrometer in the 400–4000 cm^{-1} range. Elemental analyses (C, H, N, Cl) were performed by Atlantic Microlab in Norcross, Georgia, USA. Variable-temperature dc and ac magnetic susceptibility data were collected at the University of Florida using a Quantum Design MPMS-XL SQUID magnetometer equipped with a 7 T magnet and operating in the 1.8–300 K range. Samples were embedded in solid eicosane to prevent torquing. Pascal's constants were used to estimate the diamagnetic corrections [20], which were subtracted from the experimental susceptibility to give the molar paramagnetic susceptibility (χ_M). Fitting of $\chi_M T$ vs T data was carried out using the program PHI [21].

3. Results and discussion

3.1. Syntheses

The synthetic procedure to complex **2** was similar to the previously published one for the benzoate analogue **1** [7], except that it was carried out in MeCN at 55 °C instead of $MeNO_2$ at 80 °C, which improved reagent solubilities significantly. Thus, the comproportionation reaction between MnO_4^- and Mn^{2+} in the presence of Ce^{3+} and 2-Cl-$PhCO_2H$ in a 1:4:4:32 M ratio, respectively, in MeCN at 55 °C gave a dark brown solution from which was subsequently isolated **2**·$^5/_2$MeCN as brown crystals. The MnO_4^-:Mn^{2+} ratio of 1:4 gives a Mn^{3+} average oxidation state in the reaction, and the excess

Table 1
Crystallographic and structure refinement data for **2**·$^5/_2$MeCN.

Parameters	**2**·$^5/_2$MeCN
Formula	$C_{131}H_{85.9}Ce_3Cl_{15.3}Mn_8N_{2.5}O_{46}$
FW ($g.mol^{-1}$)[a]	3833.23
Space group	$P\bar{1}$
a (Å)	15.781(2)
b (Å)	18.915(3)
c (Å)	24.196(4)
α (°)	96.989(3)
β (°)	95.833(3)
γ (°)	90.862(3)
V (Å^3)	7129.0(19)
Z	2
ρ_{calc} ($g.cm^{-3}$)	1.786
T (K)	100(2)
Wavelength (Å)	0.71073
$R1$[b,c]	0.0806
$wR2$[b,d]	0.1842

[a] Including solvent molecules.
[b] $I > 2\sigma(I)$.
[c] $R_1 = \Sigma(||Fo| - |Fc||)/\Sigma|Fo|$.
[d] $wR_2 = [\Sigma[w(Fo^2 - Fc^2)^2]/\Sigma[w(Fo^2)^2]]^{1/2}$.

of 2-Cl-$PhCO_2H$ was to avoid precipitates of Mn oxides and provide 2-Cl-$PhCO_2^-$ ligands; similar strategies have previously been employed to make other Mn/Ce heterometallic clusters [22,23]. The excess of 2-Cl-$PhCO_2H$ was also expected to prevent products containing both 2-$ClPhCO_2^-$ and $PhCO_2^-$ ligands, but **2** nevertheless contained both, and so the characterization of **2** was carried out.

3.2. Description of structure

A stereoview of the complete structure of **2** and its labeled core are shown in Fig. 1, selected bond distances in Table S1, and a space-filling representation of the complete structure in Fig. S1. The structure of **2** is very similar to that of **1** [5]. There is a $[Ce_3Mn_8(\mu_4\text{-}O^{2-})_4(\mu_3\text{-}O^{2-})_4]^{18+}$ core consisting of a tetragonally-elongated $\{Mn^{III}_8(O^{2-})_8\}$ cube (cuboid) at the center of which is the Ce^{IV} attached to the eight O^{2-} ions. On each of two opposite faces of the cube there is a Ce^{III} ion attached to two O^{2-} ions, which become μ_4. The Mn^{III}, Ce^{IV} and Ce^{III} coordination numbers are six, eight and nine, respectively, and their oxidation states were confirmed by bond valence sum (BVS) calculations (Table 2). Peripheral ligation about the resulting $[Ce_3Mn_8O_8]$ core is provided by eighteen carboxylate groups, ~15 of them being 2-Cl-benzoates that are disordered over all 18 carboxylate positions as described above, and two terminal H_2O ligands, one each on the external Ce^{III} atoms. Ignoring the disordered 2-Cl-Ph rings, the cluster has virtual D_{2h} symmetry.

The tetragonal elongation of the Mn_8 cube is assigned primarily to the disposition of the Mn^{III} Jahn-Teller elongation axes (blue bonds in Fig. 1), which greatly increase the Mn···Mn separations between the top and bottom Mn_4 subunits (Mn···Mn = 4.820(3)–4.911(3) Å) compared with those within each Mn_4 (Mn···Mn = 3.150(3)–3.325(3) Å) and prevent them being able to be bridged by additional O^{2-} ions. Thus, each of the four Mn-Mn edges between the two Mn_4 subunits is instead bridged by a carboxylate group, which becomes μ_3 by also attaching to an external Ce^{III}. Tetragonal distortions are also known for perovskites, but of a lesser magnitude that allows all edges to still be bridged by O^{2-} ions (Fig. 2a). The MnO_6 octahedra are tilted, which allows the bridging O^{2-} ions in the core to move off the Mn–Mn edges and toward the center of the cube to optimize Ce–O bond lengths (Fig. 2b). This situation is reminiscent of the orthorhombic structure of the perovskite $LnMnO_3$ manganites, where a distortion involving tilting of the MnO_6 octahedra (by an amount that depends on the Ln ionic radius) away from the high-symmetry cubic structure similarly arises from the combined effect of Mn^{III} JT distortions and a mismatch of the Ln–O and Mn–O bond lengths, moving the oxide ions off the Mn–Mn edges [24]. The $CeMn_8$ core of **2** (and **1**) can thus be fairly accurately described as the repeating unit of a lower-symmetry perovskite lattice obtained in molecular

Table 2
Bond valence sums[a] for Ce and Mn atoms in complex **2**.

Atom	Mn(II)	Mn(III)	Mn(IV)
Mn1	3.25	**2.98**	3.13
Mn2	3.26	**2.99**	3.13
Mn3	3.16	**2.89**	3.04
Mn4	3.04	**2.78**	2.92
Mn5	3.24	**2.96**	3.11
Mn6	3.21	**2.94**	3.08
Mn7	3.23	**2.95**	3.10
Mn8	3.19	**2.92**	3.07
Atom		Ce(III)	Ce(IV)
Ce1		4.23	**3.78**
Ce2		**2.99**	2.67
Ce3		**3.02**	2.69

[a] The bold value is the closest to the charge for which it was calculated. The oxidation state is the nearest whole number to this value.

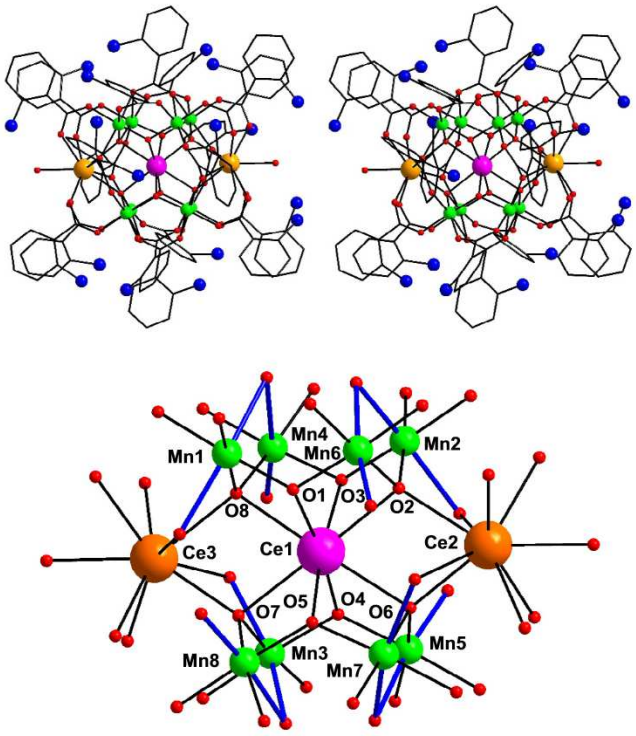

Fig. 1. A stereopair of the complete structure of complex **2**, and its labeled core; H atoms have been omitted for clarity. Color code: Mn^{III} green, Ce^{IV} purple, Ce^{III} brown, O, red; Cl, blue; C, gray. (For interpretation of the references to colour in this figure legend, the reader is referred to the web version of this article.)

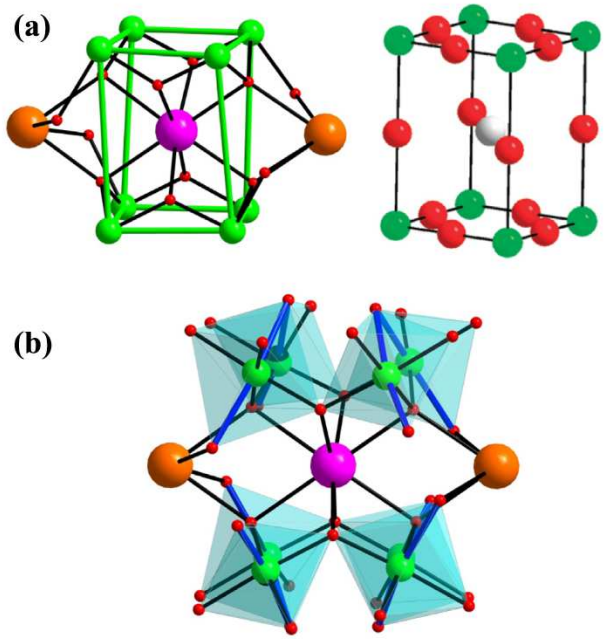

Fig. 2. **(a)** The core of complex **2** with green Mn-Mn vectors added as guides to emphasize the tetragonally-elongated Mn_8 cube (left), and its relation to a repeating unit of a tetragonally-distorted perovskite (right: adapted from [27]). **(b)** The core showing the MnO_6 octahedra to emphasize their tilting. Color code: Mn^{III} green, Ce^{IV} purple, Ce^{III} brown, O, red. (For interpretation of the references to colour in this figure legend, the reader is referred to the web version of this article.)

form. In fact, as stated elsewhere [25], the two Ce^{III} ions are at positions that in a perovskite would be in the adjacent repeating units, and thus the complete core comprises one whole and two partial repeating units. The distorted structure and decreased O^{2-} ion content suggest that these molecular species may best be considered analogues surface repeating units of perovskite nanoparticles, where structural relaxation effects and oxide ion vacancies would be present.

A closer structural comparison between **1** and **2** (Table 3) shows that the cores are essentially superimposable within uncertainties. The differences in average values of Mn-O-Mn angles (~0.6°) probably do reflect some perturbation of the core from accommodating the 2-Cl substituents (Fig. S1). In any event, since exchange couplings can be acutely sensitive to even small changes in bridging angles, even such very small structural perturbations might still lead to noticeable changes in magnetic properties, and this possibility is explored below.

3.3. Magnetochemistry

Variable-temperature dc and ac magnetic susceptibility data for vacuum-dried **2** in a 0.1 T field and in the 5.0–300 K temperature range were collected on a crushed microcrystalline sample restrained in eicosane to prevent torquing. The obtained data are plotted as $\chi_M T$ vs T shown in Fig. 3, where they are also compared with the previously reported data for **1** [7]. $\chi_M T$ at 300 K for **1** and **2** are 26.80 and 28.99 cm^3 K mol^{-1}, respectively. These are greater than the 25.62 cm^3 K mol^{-1} calculated for eight Mn^{III} (S = 2, $\chi_M T$ = 3.0 cm^3 K mol^{-1} with g = 2.0) and two Ce^{III} (f^1, S = ½, L = 3, $^2F_{5/2}$, $\chi_M T$ = 0.81 cm^3 $Kmol^{-1}$) non-interacting ions [26], indicating the strongest interactions in the complexes to be ferromagnetic (**F**). $\chi_M T$ continues to increase with decreasing T reaching peak maxima at 30 K of 32.68 and 43.81 cm^3 K mol^{-1} for **1** and **2**, respectively, and then decreases with decreasing T to 12.41 and 14.34 cm^3 K mol^{-1}, respectively, at 5.0 K due to weaker antiferromagnetic (**AF**) interactions becoming significant vs thermal energy.

As described previously, the $\chi_M T$ vs T data for **1** indicate a **C-type AF** ground state, i.e., **F** interactions in one direction and **AF** in the other two (Fig. 4). The **F** interactions in four Mn^{III}_2 pairs being the strongest in the complex explains the increasing $\chi_M T$ with decreasing T, and if they were the only interactions then $\chi_M T$ would plateau at the value for four non-interacting S = 4 units (40 cm^3 K mol^{-1} with g = 2.0) and two Ce^{III} ions, i.e. 41.60 cm^3 K mol^{-1} (dashed line in Fig. 3) – or ~39 cm^3 K mol^{-1} since g < 2 slightly for Mn^{III}. This is consistent with the increasing $\chi_M T$ for **1** but then the **AF** interactions cause it instead to peak and decrease to 12.41 cm^3 K mol^{-1} at 5.0 K.

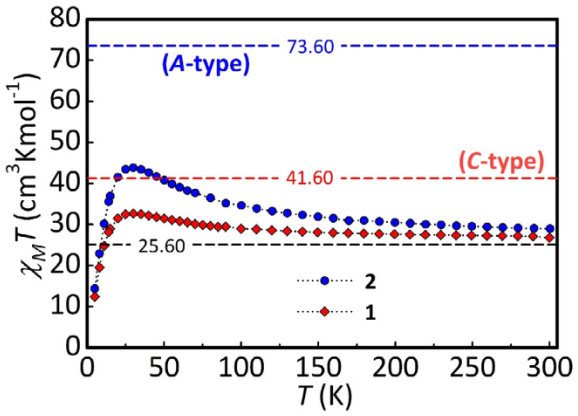

Fig. 3. $\chi_M T$ vs T plots for complexes **1** and **2** in a 1 kG (0.1 T) dc field. The Ce^{III} contributions have not been subtracted.

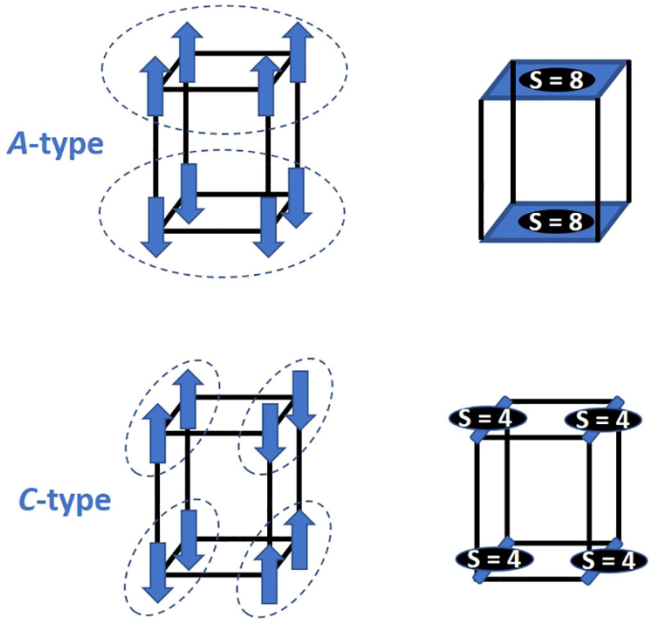

Fig. 4. Diagrammatic representation of the **A-type AF** and **C-type AF** spin configurations of an Mn^{III}_8 cube, and the resulting spins of their Mn^{III}_4 and Mn^{III}_2 units, respectively.

Table 3
Comparison of selected Mn-O-Mn angles (°) in complexes **1** and **2**.

Parameter	2	1
Mn-O_{ox}-Mn[a]	110.6(3)	110.58(12)
	111.5(3)	111.03(12)
	111.8(3)	111.12(12)
	112.7(3)	112.19(12)
average	111.7	111.23
Mn-O_{ox}-Mn[b]	123.8(3)	125.69(13)
	124.3(3)	125.19(13)
	126.4(3)	125.98(14)
	126.3(3)	126.36(14)
average	125.2	125.81
Mn-O_{car}-Mn[c]	82.8(3)	82.94(9)
	89.6(3)	88.05(10)
	86.5(3)	85.29(9)
	86.3(3)	86.68(10)
average	86.3	85.74

[a] O_{ox} = μ_4-oxide ions.
[b] O_{ox} = μ_3-oxide ions.
[c] O_{car} = μ_4-carboxylate groups.

The distinctly different $\chi_M T$ vs T for **2** is thus very interesting. Its $\chi_M T$ is by 50 K already greater than the maximum possible for a C-type **AF** ground state and appears to be extrapolating to ~50 cm^3 K mol^{-1} before **AF** interactions cause it to peak and decrease at lower T. Since we had seen from DFT calculations on **1** that the lowest-energy excited states are **A-type AF** (Fig. 4) due to **AF** $|J_3|$ being only slightly stronger than the **F** $|J_2|$ (Fig. 5), giving the antiparallel alignment of Mn^{III}_2 S = 4 spin vectors within each Mn_4 unit, a likely and feasible rationalization of the $\chi_M T$ vs T for **2** is that perturbation of the structure by the Cl substituents has caused an **A-type AF** excited state to be lower-lying than in **1** and maybe even the new ground state. For example, the spin-only (g = 2.0) $\chi_M T$ for degenerate **C-type** and **A-type AF** states would be 56 cm^3 K mol^{-1} if there were no **AF** interactions between their **F** Mn^{III}_2 pairs or **F** Mn^{III}_4 planes, respectively.

To probe this further, the $\chi_M T$ vs T plots, with the Ce^{3+} contributions of 1.60 cm^3 K mol^{-1} subtracted, were fit with program PHI [21] to the 4-J exchange-coupling model in Fig. 5 based on the spin

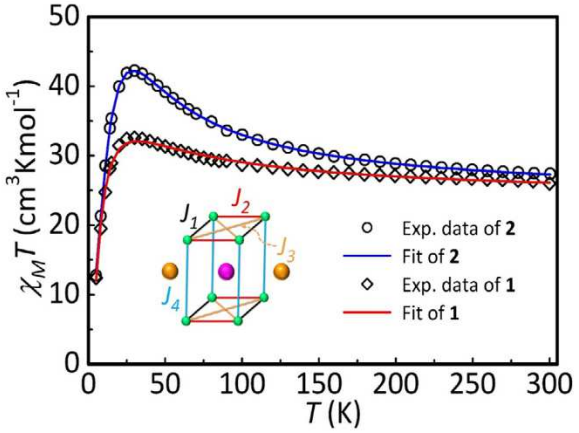

Fig. 5. Fits of the $\chi_M T$ vs T data for complexes **1** and **2** in a 1 kG (0.1 T) dc field with the contributions from their two Ce^{III} atoms subtracted. The inset shows the 4-J model employed. See Table 4 for the fit parameters.

Hamiltonian of Eq. (1). The obtained fits for **1** and **2** (solid lines in Fig. 5) gave the values of J_1–J_4 in Table 4. Those for **1** are similar to those previously reported [7], and the most significant difference for **2** is that its **AF** $|J_3|$ is now found to be slightly weaker than **F** $|J_2|$. If this

$$H = -2J_{ij}\Sigma\hat{S}_i \cdot \hat{S}_j \quad (1)$$

is the case, then the net interaction between the two **F** Mn_2^{III} pairs in each Mn_4 unit would be **F** and an **A-type AF** ground state would result. However, this conclusion depends on the accuracy/reliability of the fit parameters for **2**, and this point will be discussed further below.

To explore the low-T regime in the absence of an applied field, ac magnetic susceptibility data were collected on **2** at 1.8–15 K in a 3.5 G ac field at a 1000 Hz oscillation frequency. The in-phase ac susceptibility (χ'_M) as $\chi'_M T$ vs T (Fig. 6) shows a steeply decreasing $\chi'_M T$ with decreasing T below 15 K consistent with very low-lying excited states resulting from the very weak J_4 couplings between the top and bottom Mn_4 units. Extrapolation of the plot to 0 K gives a small value consistent with two non-interacting Ce^{III} ions (1.60 cm^3 K mol^{-1}). Thus, at very low T the complex behaves as a $Ce^{IV}Mn_8^{III}$ cluster in its S = 0 ground state and two independent Ce^{III} ions. As expected, no out-of-phase χ''_M signal (Fig. S2) was observed, indicating the absence of slow magnetization relaxation at ≥1.8 K in **2** consistent with the S = 0 ground state.

3.4. Feasibility of a change in the ground state spin

The above data augur well for the objective of accomplishing a ground state spin change in these Ce_3Mn_8 complexes, but the results to date need to be interpreted with caution. First, the procedure employed to prepare the 2-Cl-benzoate has led to a mixed-carboxylate product that shows extensive disorder of the 2-Cl-benzoate group positions and/or their Cl atom positions and occupancies. In effect, the crystals contain a large number of isomeric products with a corresponding range of structural perturbations on the cores and thus a corresponding range for each of the J

Table 4
Fit parameters[a,b] for complexes **1** and **2**.

Complex	J_1	J_2	J_3	J_4
2	+6.2	+4.4	−2.6	−0.5
1	+5.3	+3.3	−3.4	−0.1

[a] cm^{-1}.
[b] With a fixed g = 2.0.

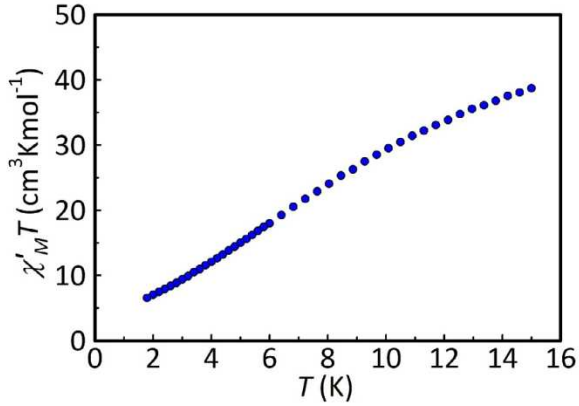

Fig. 6. In-phase ac $\chi'_M T$ vs T data for **2** in the 1.8–15.0 K range.

exchange couplings. Of course, the crystallography provides merely an average structure, and the magnetic data and their J_1–J_4 fit parameters are also averages. Nevertheless, the $\chi_M T$ vs T plot for **2** (Fig. 3) and the fit parameters in Table 4 clearly show, we believe, that the **C-type** and **A-type AF** states are much closer together than in **1**. However, we worry about the intrinsic uncertainties and the isomeric ranges in the obtained J_1–J_4 for **2**, and thus we do not feel justified to claim that the ground state has changed. It could even be possible that the sample consists of some molecules with **C-type** and some with **A-type AF** ground states, depending on the degree of their structural perturbation.

These caveats notwithstanding, we are encouraged that the approach of introducing substituents into the benzoate groups to target ligand-induced structural perturbation of the core and resulting changes to the magnetic properties seems to be working. The next objectives in the project are quite clear: (i) we must develop synthetic procedures that yield complexes with all ligands containing the bulky substituent to minimize isomeric forms; (ii) we must target greater structural perturbation so that not only might the ground state clearly change but it would be sufficiently separated in energy from the lowest excited states that the magnetic data show unequivocally an **A-type AF** ground state; and (iii) we must expand the project to include additional probes of the magnetic structure such as inelastic neutron scattering. All these efforts are in progress.

4. Conclusions

Introduction of a Cl atom into the benzoate ligands of **1** to introduce 'chemical pressure' has been found to cause a small structural perturbation of the core and a distinct change in the magnetic properties as evidenced by the significantly different $\chi_M T$ vs T plots for **1** and **2**. Although we cannot conclude on the basis of available data that the ground state has changed to **A-type AF**, the results nevertheless provide a valuable proof-of-feasibility of this approach. We thus feel confident that it may prove possible using these molecular analogues of the perovskite repeating unit to demonstrate the ground state spin switching predicted by the theoretical studies described in the introduction [8,9]. This also provides another point of emphasis for the contribution that the molecular approach can provide as a bottom-up approach to the study of ultra-small nanoparticles of important metal oxides. Further studies are in progress.

CRediT authorship contribution statement

Thai Son Cao: Methodology, Investigation, Writing - original draft. **Dian-Teng Chen:** Validation. **Khalil A. Abboud:** Formal

Analysis. **Xiaoguang Zhang:** Validation. **Hai-Ping Cheng:** Validation. **George Christou:** Conceptualization, Supervision, Writing - original draft, Writing - review & editing.

Declaration of Competing Interest

The authors declare that they have no known competing financial interests or personal relationships that could have appeared to influence the work reported in this paper.

Acknowledgement

This work was supported by the USA National Science Foundation by grant NSF/DMREF CHE-1534401.

Appendix A. Supplementary data

Supplementary data to this article can be found online at https://doi.org/10.1016/j.poly.2019.114275.

References

[1] A. Trovarelli, Catal. Rev. 38 (1996) 439–520.
[2] Q. Wang, B. Zhao, G. Li, R. Zhou, Environ. Sci. Technol. 44 (2010) 3870–3875.
[3] X. Qi, M. Flytzani-Stephanopoulos, Ind. Eng. Chem. Res. 43 (2004) 3055–3062.
[4] S. Sharma, S. Hilaire, J.M. Vohs, R.J. Gorte, H.-W. Jen, J. Catal. 190 (2000) 199–204.
[5] E. Perry Murray, T. Tsai, S.A. Barnett, Nature 400 (1999) 649–651.
[6] K.J. Mitchell, K.A. Abboud, G. Christou, Nature Commun. 8 (2017) 1445.
[7] A.E. Thuijs, X.-G. Li, Y.-P. Wang, K.A. Abboud, X.-G. Zhang, H.-P. Cheng, G. Christou, Nature Commun. 8 (2017) 500.
[8] R. Maezono, S. Ishihara, N. Nagaosa, Phys. Rev. B 58 (1998) 11583–11596.
[9] T. Hotta, S. Yunoki, M. Mayr, E. Dagotto, Phys. Rev. B 60 (1999) 15009–15012.
[10] B.R.K. Nanda, S. Satpathy, J. Magn. Magn. Mater. 322 (2010) 3653–3657.
[11] P. Rivero, V. Meunier, W. Shelton, Phys. Rev. B 93 (2016) 094409.
[12] I. Loa, P. Adler, A. Grzechnik, K. Syassen, U. Schwarz, M. Hanfland, G.Kh. Rozenberg, P. Gorodetsky, M.P. Pasternak, Phys. Rev. Lett. 87 (2001) 12550.
[13] L. Pinsard-Gaudart, J. Rodríguez-Carvajal, A. Daoud-Aladine, I. Goncharenko, M. Medarde, R.I. Smith, A. Revcolevschi, Phys. Rev. B 64 (2001) 064426.
[14] M. Baldini, T. Muramatsu, M. Sherafati, H.-K. Mao, L. Malavasi, P. Postorino, S. Satpathy, V.V. Struzhkin, Proc. Natl. Acad. Sci. 112 (2015) 10869–10872.
[15] M. Murugesu, M. Habrych, W. Wernsdorfer, K.A. Abboud, G. Christou, J. Am. Chem. Soc. 126 (2004) 4766–4767.
[16] T.C. Stamatatos, K.A. Abboud, W. Wernsdorfer, G. Christou, Angew. Chem. 119 (2007) 902–906.
[17] T.C. Stamatatos, D. Foguet-Albiol, K.M. Poole, W. Wernsdorfer, K.A. Abboud, T. A. O'Brien, G. Christou, Inorg. Chem. 48 (2009) 9831–9845.
[18] SAINT, Bruker-AXS: Madison, WI., USA, (2013).
[19] SHELXTL2014, Bruker-AXS: Madison, Wisconsin, USA, (2014).
[20] G.A. Bain, J.F. Berry, J. Chem. Educ. 85 (2008) 532.
[21] N.F. Chilton, R.P. Anderson, L.D. Turner, A. Soncini, K.S. Murray, J. Comput. Chem. 34 (2013) 1164–1175.
[22] A.E. Thuijs, A. Marton, T.C. Stamatatos, K.A. Abboud, G. Christou, Polyhedron 103 (2016) 288–294.
[23] C. Papatriantafyllopoulou, K.A. Abboud, G. Christou, Polyhedron 52 (2013) 196–206.
[24] M. Tachibana, T. Shimoyama, H. Kawaji, T. Atake, E. Takayama-Muromachi, Phys. Rev. B 75 (2007) 144425.
[25] R.J.D. Tilley, Perovskites: Structure–Property Relationships, John Wiley & Sons, ltd., 2016, ISBN: 9781118935668.
[26] O. Kahn, Molecular Magnetism, VCH Publishers, Inc., 1993, ISBN: 1-56081-566-3.
[27] E. Dixon, J. Hadermann, S. Ramos, A.L. Goodwin, M.A. Hayward, J. Am. Chem. Soc. 113 (2011) 18397–18405.